Available online at www.sciencedirect.com
ScienceDirect
International Journal of Heat and Mass Transfer 50 (2007) 4387–4399
International Journal of HEAT and MASS TRANSFER
www.elsevier.com/locate/ijhmt

Modelling the pyrolysis of wet wood – II. Three-dimensional cone calorimeter simulation

R.K.K. Yuen [a], G.H. Yeoh [b,*], G. de Vahl Davis [c], E. Leonardi [c]

[a] Department of Building and Construction, City University of Hong Kong, Tat Chee Avenue, Kowloon, Hong Kong
[b] B40, Australian Nuclear Science and Technology Organisation (ANSTO), PMB 1, Menai, NSW 2234, Australia
[c] School of Mechanical and Manufacturing Engineering, University of New South Wales, NSW 2052, Australia

Received 24 March 2006; received in revised form 6 January 2007
Available online 2 May 2007

Abstract

Application of a three-dimensional mathematical model for the pyrolysis of wet wood coupled with the gas phase combustion to the analysis of a wood sample ignited in a cone calorimeter is described. Time-dependent chemical and physical processes of wet wood model described in Part I is employed with transient gas phase flow described by Navier–Stokes equations. Predicted ignition times compared well against experimental data for cone irradiation fluxes of 20–70 kW m^{-2} with initial moisture contents of 0%, 5% and 10%. This study further demonstrates the feasibility of application of the developed wet wood model in fire-engineering.

Keywords: Cone calorimeter; Wet wood pyrolysis; Gas phase combustion; Cone irradiation fluxes

1. Introduction

The cone calorimeter apparatus is an industrial standard for testing of materials (ASTM E1354 [1], ISO 5660 [2]). It provides the necessary means of measuring the mass-loss rates, heat-release rates, ignitability, and visible smoke production in a wide variety of materials under controlled levels of radiant heating. Fig. 1a depicts a schematic view of the apparatus, which consists of a conical heater providing controlled levels of irradiance to a solid specimen located under the cone while Fig. 1b illustrates the boundary conditions imposed for the computational model, which will be further discussed later. The heater is designed to offer a uniform irradiance on a horizontal surface where the test specimen is placed. Thermal radiation from the conical heater induces pyrolysis in the test specimen. Inflammable gases are released and make their way to the solid surface. A buoyancy-driven flow in the cone is established due the radiation and combustion heat upon ignition. For piloted ignition tests, an electric spark (the pilot) is usually located above the sample within the experimental apparatus. It is applied at regular intervals above the surface of the pyrolysing material and ignition is initiated providing the local mixture ratio is near or within the flammability limits. The apparatus allows the time for spontaneous and piloted ignition of the material exposed to the different irradiance levels to be assessed. Also, the rate of heat release of the combustible solid can be determined by the assessment of the oxygen depletion rate.

Some important investigations demonstrating the versatility of the cone calorimeter for obtaining the flammability characteristics of charring and non-charring materials are briefly mentioned. Peacock et al. [3] have evaluated interior finishing materials of a broad cross section of Amtrak passenger train cars in the cone calorimeter to determine whether the tested materials met the current Federal Railroad Administration fire safety guidelines. Tsai and Drysdale [4] have demonstrated the use of the quantitative

* Corresponding author. Tel.: +61 2 9717 3817; fax: +61 2 9717 9263.
E-mail address: Guan.Yeoh@ansto.gov.au (G.H. Yeoh).

0017-9310/$ - see front matter © 2007 Elsevier Ltd. All rights reserved.
doi:10.1016/j.ijheatmasstransfer.2007.01.018

Nomenclature

A_i^k, A_j^k, A_i^l	adjugate Jacobian metric elements
A	pre-exponential constant in Arrhenius equations
C_p	specific heat capacity
D	mass diffusivity
E	activation energy in Arrhenius equations
F	gas volatiles
$F_{\text{w-c}}$	shape factor from wood sample to the cone
$F_{\text{w-o}}$	shape factor from wood sample to the surroundings
g_i	gravity
g^{lm}	contravariant metric tensor elements
$\sqrt{g}$	Jacobian determinant
Gr	Grashof number
h	enthalpy
h_{t}, h_{b}	vertical distances of the top and bottom of the cone from the wood
m''	mass flux
M	molar mass
n	normal direction to boundary surface
O	oxidant
p	pressure
P	products
P_{o}	atmospheric pressure
r_{t}, r_{b}	radii of the top and bottom of the cone
s	horizontal distance of P from the central axis
R_{g}	combustion rate of fuel
R_{u}	universal gas constant
t	time
T	temperature
u_i	velocity
u, v, w	velocity components along the Cartesian directions
$\widehat{U}^l$	normal flux components if the velocity vector
Y_{m}	mass fraction of species m

Greek symbols

β_{kl}	geometric coefficients of the non-orthogonal curvilinear transformation
ε	surface emissivity
λ	thermal conductivity
μ	dynamic viscosity
ρ	density
σ	Stefan–Boltzmann constant
σ_{h}, σ_{Y}	Prandtl/Schmidt number
υ	number of moles of the gas species
ξ^l	lth non-orthogonal coordinate

Subscripts

c	carbon dioxide, cone
g	fuel/gas volatiles
o	oxidant, ambient condition
s	solid phase within the virgin wood
so	wood surface
v	vapour
w	virgin wood

data obtained from the cone calorimeter to effectively model upward spread of flame on flat vertical combustible surfaces. Non-charring polymeric material such as polymethylmethacrylate (PMMA) was employed as the pyrolysing fuel specimen. Recently, Delichatsios et al. [5] conducted extensive cone calorimeter experiments to determine the flammability properties of charring material based on Australian radiata pine. The deduced properties were applied for the prediction of ignition and pyrolysis histories of wood. Many empirical or semi-empirical models have been developed to predict flame spread and room corner fire growth on wall linings on the basis of ignition, heat and smoke release data obtained through the cone calorimeter experiments.

A number of mathematical models have been developed in the specific area of the cone calorimeter. Theoretical studies on the burning of polymeric material such as PMMA can be found in notable works [6–11]. An integral model, essentially a one-dimensional (1D) pyrolysis model, has been developed by Moghtaderi et al. [12,13] to study the transient pyrolysis of charring materials. Recently, Spearpoint and Quintiere [14] employed the integral method to describe the transient pyrolysis of semi-infinite charring solids of various species subjected to constant radiant heat fluxes with different grain orientations. The time to ignition measurements obtained from the cone calorimeter were used to derive the characteristic material properties, which were used as input to the model. Nevertheless, for simulation of fire growth and spread in enclosures, the 1-D integral model for wood pyrolysis cannot truly represent boundary conditions of actual geometrical structures.

Previous analysis of wood combustion in the cone calorimeter using computational fluid dynamics (CFD) has been presented by Novozhilov et al. [15]. This paper dealt with the description of the coupling between the CFD-based field model incorporating turbulence, combustion, radiation and soot formation and a solid pyrolysis model for the burning of wood. They have applied a very simple pyrolysis model without the consideration of accounting for the anisotropic, hygroscopic and kinetic properties of wood. The wood sample was therefore assumed to be dry and all volatiles escaped as soon as they were formed. Based on the investigation in Part I of these two part study on modeling pyrolysis of wet wood, these assumptions have been found not to be strictly true. Furthermore, their analysis focused more on the burning characteristics after ignition.

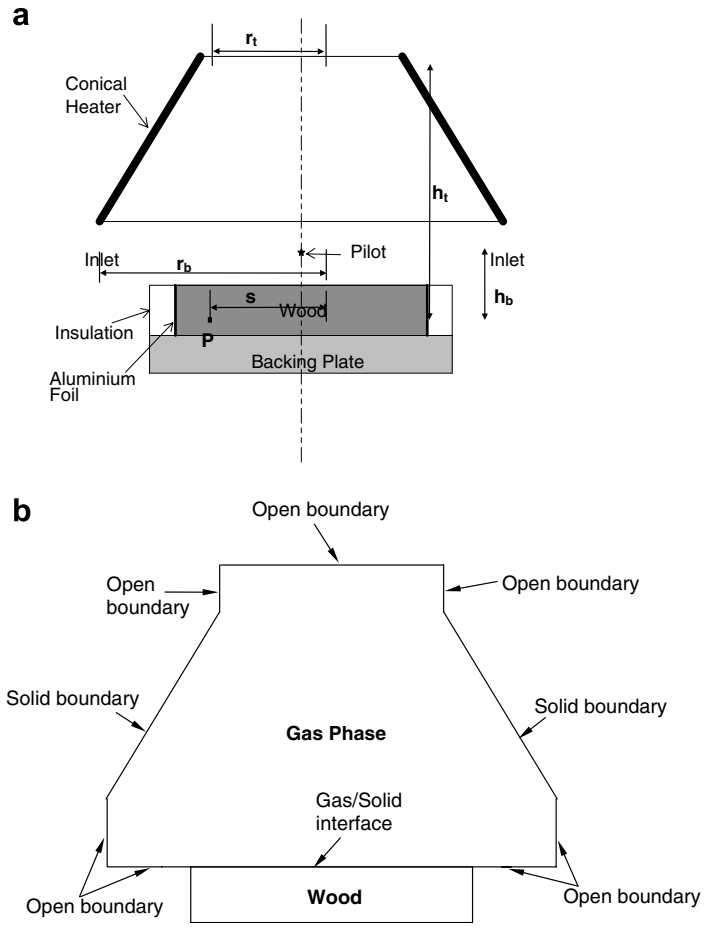

Fig. 1. Cone calorimeter: (a) Physical model of the wood combustion and (b) boundary conditions in the gas phase and the gas/solid interface.

The present contribution in this paper employs a three-dimensional field model to solve a time-dependant, full (elliptic) form of the Navier–Stokes equations. This model uses a non-orthogonal, curvilinear coordinate system, making the model applicable to a wide range of geometries. Previously, we have applied the model to simulate the heat-transfer, pyrolysis, fuel–air mixing, and pilot ignition of a PMMA fuel sample within the cone calorimeter [10]. A three-dimensional grid was generated to form the axi-symmetric flow field within the cone, including the solid fuel sample under the cone, and the surrounding inlet and exit flow regions. The same model is adopted for the current study. A transient pyrolysis model is included so that the detailed ignition process within the cone calorimeter could be studied – the primary investigation in further assessing the developed pyrolysis model in Part 1 in this second part of a three-dimensional simulation in a cone calorimeter environment. A numerical treatment for the simulation of the pilot ignition is included. The irradiances from the conical heater on to the wood surface are calculated analytically in the computations. Temperature–time histories of the wood and of the gases above the wood that illustrate the pre-combustion, ignition and combustion phases of the process are presented. The computed field variables including the temperature, pressure, mass fluxes, char and moisture content in the pyrolysing wood as well as the temperature, velocity, and the concentration of species in the gas phase are discussed including the effects of variations in the initial moisture content of wood. The predicted ignition times are compared with experimentally determined values by Shields et al. [16]. In this study, radiative heat transfer between the cone and fuel surface has been included in the model, however, the participation of the gas phase in the radiation heat transfer has been neglected. Since the modelled cone calorimeter used a pilot ignitor, it was evident that the gas-phase radiation would not play a major part in the ignition process.

2. Computational model

2.1. Solid phase

The formulation of a 3-D pyrolysis model incorporating the moisture content, anisotropic properties of wood and the internal convection of gases have been presented in detail in Part I of this two part study. To reiterate the salient features of the model, the pyrolysis process was assumed to obey an Arrhenius equation. An enthalpy equation, which accounted for conduction, internal convection due to the movement of combustible gases and

water vapour inside the burning wood and heats of pyrolysis and evaporation, was formulated. Consideration was also taken to conserve the mass for both the water vapour and chemical species. Evaporation process of moisture inside the wood was handled through a consideration of the saturation vapour pressure. The transport of combustible gases and water vapour through the charring solid was assumed to obey Darcy's Law. The anisotropic nature of the material was particularly included and the properties of the charring wood were assigned the extent-of-reaction and temperature dependence. Thermal swelling, shrinkage, surface regression and possible surface oxidation reactions of the virgin wood and char have not been modelled. This approach is valid during the initial stages of pyrolysis and ignition process of wood. However, as burning proceeds, further morphological changes such as cracking may result in less resistance on the combustible volatile gases escaping from the wood. In such a case, the current model may under-predict the emission rates of the volatile gases.

2.2. Gas phase

The gas phase combustion equations comprise of the conservation of mass, momentum, energy, and chemical species. These equations have also been transformed into non-orthogonal coordinates, consistent with the governing equations describing the wet wood pyrolysis, and they are given as:

Continuity

$$\frac{\partial \rho}{\partial t}+\frac{1}{\sqrt{g}}\frac{\partial}{\partial \xi^l}\left(\rho \widehat{U}^l\right)=0 \tag{1}$$

Momentum

$$\begin{aligned}\frac{\partial(\rho u_i)}{\partial t}=&-\frac{1}{\sqrt{g}}\frac{\partial}{\partial \xi^l}\left[\rho \widehat{U}^l u_i-\mu\sqrt{g}g^{lm}\frac{\partial u_i}{\partial \xi^m}\right]\\&-\frac{A_i^k}{\sqrt{g}}\frac{\partial}{\partial \xi^k}\left(p+\frac{2}{3}\mu\frac{1}{\sqrt{g}}\frac{\partial \widehat{U}^l}{\partial \xi^l}\right)\\&+\frac{A_j^k}{\sqrt{g}}\frac{\partial}{\partial \xi^k}\left(\mu\frac{1}{\sqrt{g}}A_i^l\frac{\partial u_j}{\partial \xi^l}\right)+(\rho-\rho_o)g_i\end{aligned} \tag{2}$$

Enthalpy

$$\frac{\partial(\rho h)}{\partial t}=-\frac{1}{\sqrt{g}}\frac{\partial}{\partial \xi^l}\left[\rho \widehat{U}^l h-\frac{\mu}{\sigma_h}\sqrt{g}g^{lm}\frac{\partial h}{\partial \xi^m}\right] \tag{3}$$

Species concentration

$$\frac{\partial(\rho Y_g)}{\partial t}+\frac{1}{\sqrt{g}}\frac{\partial}{\partial \xi^l}\left[\rho \widehat{U}^l Y_g-\frac{\mu}{\sigma_Y}\sqrt{g}g^{lm}\frac{\partial Y_g}{\partial \xi^m}\right]=-R_g \tag{4}$$

$$\frac{\partial(\rho Y_o)}{\partial t}+\frac{1}{\sqrt{g}}\frac{\partial}{\partial \xi^l}\left[\rho \widehat{U}^l Y_o-\frac{\mu}{\sigma_Y}\sqrt{g}g^{lm}\frac{\partial Y_o}{\partial \xi^m}\right]=-\frac{\upsilon_o^g M_o}{\upsilon_g M_g}R_g \tag{5}$$

$$\frac{\partial(\rho Y_c)}{\partial t}+\frac{1}{\sqrt{g}}\frac{\partial}{\partial \xi^l}\left[\rho \widehat{U}^l Y_c-\frac{\mu}{\sigma_Y}\sqrt{g}g^{lm}\frac{\partial Y_c}{\partial \xi^m}\right]=\frac{\upsilon_c^g M_c}{\upsilon_g M_g}R_g \tag{6}$$

$$\frac{\partial(\rho Y_v)}{\partial t}+\frac{1}{\sqrt{g}}\frac{\partial}{\partial \xi^l}\left[\rho \widehat{U}^l Y_v-\frac{\mu}{\sigma_Y}\sqrt{g}g^{lm}\frac{\partial Y_v}{\partial \xi^m}\right]=\frac{\upsilon_v^g M_v}{\upsilon_g M_g}R_g \tag{7}$$

where $\widehat{U}^l=\sum_{k=1}^{3}\beta_{kl}u_k$; σ_h is the Prandtl number; and σ_Y is the Schmidt number. Y_g, Y_o, Y_c and Y_v represent the mass fractions of fuel, oxygen, carbon dioxide and vapour, respectively. R_g expresses the combustion rate of the fuel and υ is the number of moles of the gas species as described in the stoichiometric equation for the complete combustion of fuel. The terms of A_i^k, A_j^k and A_i^l are the adjugate Jacobian metric elements while g^{lm} is the contravariant metric element in the non-orthogonal coordinates transformation.

The gases are assumed to obey the ideal gas law. Mixture dynamic viscosity is taken to be dependent on the local temperature while mixture specific heats are taken to be the mass averaged values. The flow field within the cone is modelled as laminar. This assumption can be examined by calculating the Grashof (Gr) number for the cone at the maximum irradiance 70 kW m^{-2} that has been investigated in the current pilot ignition study. The resulting Grashof number varied from 1.1×10^6 to 2.8×10^6 depending on reference length scale. These values are significantly below the Grashof where transition to turbulence would typically occur ($Gr\approx1\times10^8$ to 1×10^9) in free convection flow [17]. The Rayleigh number for the flow over the horizontal hot wood sample is evaluated to be approximately 1×10^5, which is still significantly lower than the corresponding Rayleigh number required for transition ($\approx1\times10^7$). The effect of heat release due to combustion on transition is at this moment uncertain, however, this effect should only become significant once ignition of the fuel/air mixture has been achieved and a turbulent flame develops, which is beyond the scope of the present study.

2.3. Interfacial considerations between the solid and gas phases

The conservation equations in the solid and gas are coupled through energy and mass balances at the interface. It was assumed from the consideration in Kuo [18] that the gas stream emerging from the solid phase was totally fuel. For wood pyrolysis, the stream of gases from the wood consists of fuel, vapour, oxygen, carbon dioxide and inert gases.

Considering the mass balance at the interface, the total mass of fuel species leaving the surface of the wood equals to the mass flux of the fuel species due the bulk velocity of the mixture and mass flux of fuel species due to the mass diffusion at the interface. The mass balance equation of fuel, vapour, oxygen and carbon dioxide at the interface can be written as:

$$\rho D\frac{\partial Y_g}{\partial n}=m^n Y_g-m_g^n \tag{8}$$

$$\rho D\frac{\partial Y_v}{\partial n} = m^n Y_v - m_v^n \tag{9}$$

$$\rho D\frac{\partial Y_o}{\partial n} = m^n Y_o \tag{10}$$

$$\rho D\frac{\partial Y_c}{\partial n} = m^n Y_c \tag{11}$$

where m^n is the total mass flux and ρ and D are the density and mass diffusivity in the gas phase.

The conservation equations in the solid and gas are coupled through energy and mass balances at the interface which can be expressed as:

$$-\lambda\frac{\partial T}{\partial n} = -\lambda_s\frac{\partial T_s}{\partial n} - F_{w-c}\varepsilon\sigma\left[T_{so}^4 - T_c^4\right] - F_{w-o}\varepsilon\sigma\left[T_{so}^4 - T_o^4\right] \tag{12}$$

where ε denotes the surface emissivity; σ is the Stefan–Boltzmann constant; T and T_s are respectively the gas and solid phase temperatures; λ and λ_s are the thermal conductivities in the gas and solid phases; T_{so} is the wood surface temperature; and T_o is the ambient temperature. The shape factors $F_{w\text{-}c}$ and $F_{w\text{-}o}$ from any point P in Fig. 1 at the upper surface of the wood to the cone and to the surroundings can be derived from expressions for standard geometrical configurations [19]. They can be formulated respectively as

$$F_{w-o} = 1 - F_{w-c} \tag{13}$$

$$F_{w-c} = \frac{1}{2}\left\{\frac{s^2 + h_t^2 - r_t^2}{\sqrt{\left(s^2 + h_t^2 + r_t^2\right)^2 - 4(sr_t)^2}} - \frac{s^2 + h_b^2 - r_b^2}{\sqrt{\left(s^2 + h_b^2 + r_b^2\right)^2 - 4(sr_b)^2}}\right\} \tag{14}$$

where s is the horizontal distance of P from the axis; h_t and h_b are the vertical distances of the top and bottom of the cone from the wood; and r_t and r_b are the radii of the top and bottom of the cone, as shown in Fig. 1.

2.4. Chemical kinetics

The complexity of the gas phase chemical reaction mechanism for the gas volatiles of wood has continued to preclude any detailed numerical analysis. A one-step global reaction remains the common way to model the combustion [20,21]. Amongst the many consensus reached based on numerous experimental works on wood, the gas volatiles has the mean molecular form of CH_2O [22]. A one-step global reaction is given by

$$CH_2O + O_2 \rightarrow CO_2 + H_2O \tag{15}$$

The finite-rate chemical kinetics can be modeled by treating the above global reaction as a second-order reaction of the form:

$$F + O \rightarrow P \tag{16}$$

where F represents the gas volatiles, O the oxidant and P the products; and evaluating the source term of the fuel from the following Arrhenius expression:

$$R_g = A\rho^2 Y_g Y_o \exp\left[-E/(R_u T)\right] \tag{17}$$

where A is the pre-exponential constant and E is the activation energy for the gas combustion reaction. The kinetic constants A and E for CH_2O have been obtained from the experiments of Westbrook and Dryer [23].

3. Numerical details

In the current study, the pilot, which is an electrical spark introduced at regular time intervals of 1 s in the cone calorimeter, has been modelled. During the numerical simulation, this pilot has been introduced by raising the temperature of the gas at the control volume located at the pilot position to a temperature of 1000 K – a condition found to be sufficient for ignition of the fuel. This heat source is initiated intermittently at regular time intervals of 1 s until sustained flaming occurs. It was demonstrated that the energy contributed by the small pilot spark in this 3-D model caused no adverse effect on the piloted ignition time. Other temperature values of 1200 K and 1500 K have been tested. The time to ignition was found to vary within a range of 1 s at the irradiance 60 kW m^{-2}. In order to limit the undue heating effects on the computed ignition time, the value of 1000 K was selected. This is in contrast with the method used by Tzeng and Atreya [18] in their one-dimensional pilot ignition model of wood. They simulated the pilot ignition source by introducing a high temperature intermittently at a position above the wood. Effectively, the pilot ignition source used was, therefore, equivalent to an infinite slab. To avoid excess heating effect to the solution domain, they had to adopt a special procedure to eliminate the heat accumulation from the slab ignition source throughout the simulation until the ignition of wood occurs. Since the pilot has been simulated numerically, the ignition criteria such as critical surface temperature and critical mass flux were not required.

The conservation equations were discretised using a control volume technique. They were solved using the Stone's Strongly Implicit Procedure [24] and the Incomplete Factorisation Conjugate Gradient solver [25] to achieve the time-dependent solutions to the systems of algebraic equations in a fully implicit fashion. A total of $13 \times 13 \times 15$ control volumes in the ξ^1 (axial), ξ^2 (circumferential) and ξ^3 (radial) directions were employed for the solid phase while $38 \times 13 \times 24$ control volumes were used for the gas phase. Fig. 2 shows the non-uniform mesh that was used in the wood and the air regions with the mesh concentrated immediately below and above the surface of the wood, to accommodate the steep gradients there. A time step of 0.05 s was used. Since the objective of this numerical study was to predict the time to piloted ignition, a sensitivity analysis of the mesh size was performed. It was found that the computed piloted ignition time remained unchanged when the above mesh sizes in the gas and solid phase were increased to $18 \times 18 \times 21$ and $52 \times 18 \times 34$, respectively

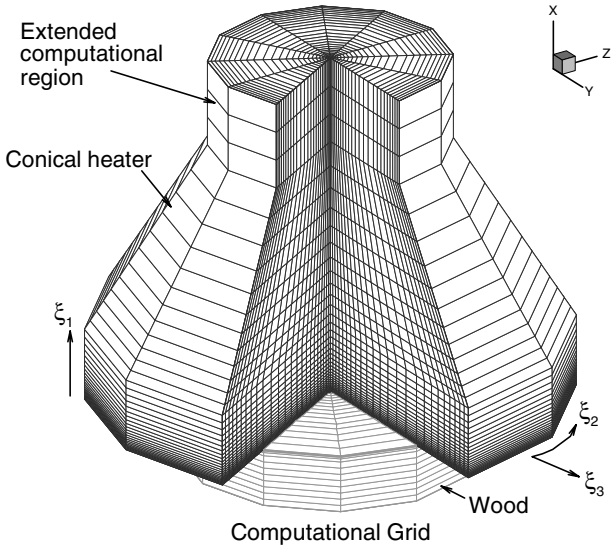

Fig. 2. The computational grid for gas phase and wood with the x-axis along the direction of grains.

for a cone irradiance of 40 kW m^{-2} and moisture content of 0%.

3.1. Boundary conditions

Fig. 1b presents the boundary conditions imposed on the computational model of the cone calorimeter configuration. At the interface between the solid and gas phases, the velocity boundary conditions are given by the mass flux of the emerging stream of volatile gases from the solid: $\rho u = m''$. The pressure may fluctuate slightly due to the flow conditions. However, the fluctuations can be taken to be relatively insignificant when compared to the pressure variations as computed inside the wood due to the evaporation of moisture and pyrolysis. The pressure at the interface was specified and taken to be at atmospheric pressure ($P_o = 1.013$ bar). For the energy equation, the boundary condition at the interface, related to the heat fluxes on the surface of wood, has been described in Eq. (12).

At the conical heater surface, no-slip condition was applied for the velocity. Neumann condition was specified for the species mass fractions where their normal gradients at the boundary were zero while for the temperature, constant heat flux values were imposed.

At the open boundaries, there were two typical types of boundary conditions: inflow and outflow boundaries, depending on the direction of the flow. For an inflow boundary, the values of the velocity components u, v and w were specified. The temperature and mass fraction of species were given by the upstream (ambient) values. Outflow boundaries were often located at positions where flows were unidirectional and stresses were known. The pressure was specified to be at atmospheric pressure. Adopting the Neumann condition, the gradients of the velocity, temperature and mass fractions of species have all be assumed to be zero. Pressure boundary conditions were applied to the inlet and outlet boundaries. Fixed pressures were specified at the open boundaries and source and sink terms were formulated on the boundary to give the correct mass flow into and out of the constant pressure boundaries.

3.2. Property values

The physical properties and parameters employed have been described in Part I of this two-part study. These values were compiled from data presented previously by Alves and Figueiredo [26], Fredlund [27] and Di Blasi [28]. The initial temperature of the wood was set to 23 °C which corresponded to the standard conditions of the cone calorimeter tests. In this study, the wood geometry corresponded to the wood samples of various initial moisture contents in the form of a circular block with a diameter of 100 mm and a thickness of 45 mm that were irradiated and qualitatively studied in the cone calorimeter experiments. Based on the experimental observations, the surface of the wood was taken to be gray, which the surface emissivity was assumed to be 0.8 [19].

4. Results and discussion

The three-dimensional model, comprised both the wood pyrolysis and gas phase flaming combustion, has been used to simulate the piloted ignition and burning of wood in a cone calorimeter configuration. During the simulations, cone irradiances of 20, 40, 60 and 70 kW m^{-2}, correspond to fires of different magnitudes, were used. In order to investigate the effects of moisture content of wood on piloted ignition and combustion, initial moisture contents of 0%, 5% and 10% were considered. The computed transient results at various irradiances and initial moisture contents are presented and discussed below.

4.1. Prediction of piloted ignition time

The prediction of piloted ignition time for a particular irradiance and initial moisture content of wood was obtained from the computed temperature history at the pilot position. Fig. 3 shows the transient temperature evolution at the pilot position of different irradiance levels and initial moisture contents.

For dry wood (0% initial moisture content), the ignition time for the irradiance level at 40 kW m^{-2} was predicted to be 8 s. Burning was ascertained to be sustained after ignition. For wet wood with 5% and 10% initial moisture content, it was observed that flashing (unsustained ignition) occurred at 9 and 11 s. However, combustion could not be sustained and the flame was extinguished within 2–3 s due to an insufficient supply of fuel from the wooden specimen. The pilot was turned off when flashing began, but was initiated again once it ceased. Sustained combustion was eventuated for both cases of moisture contents of 5% and 10%, at 15 and 20 s, respectively. Not surprisingly,

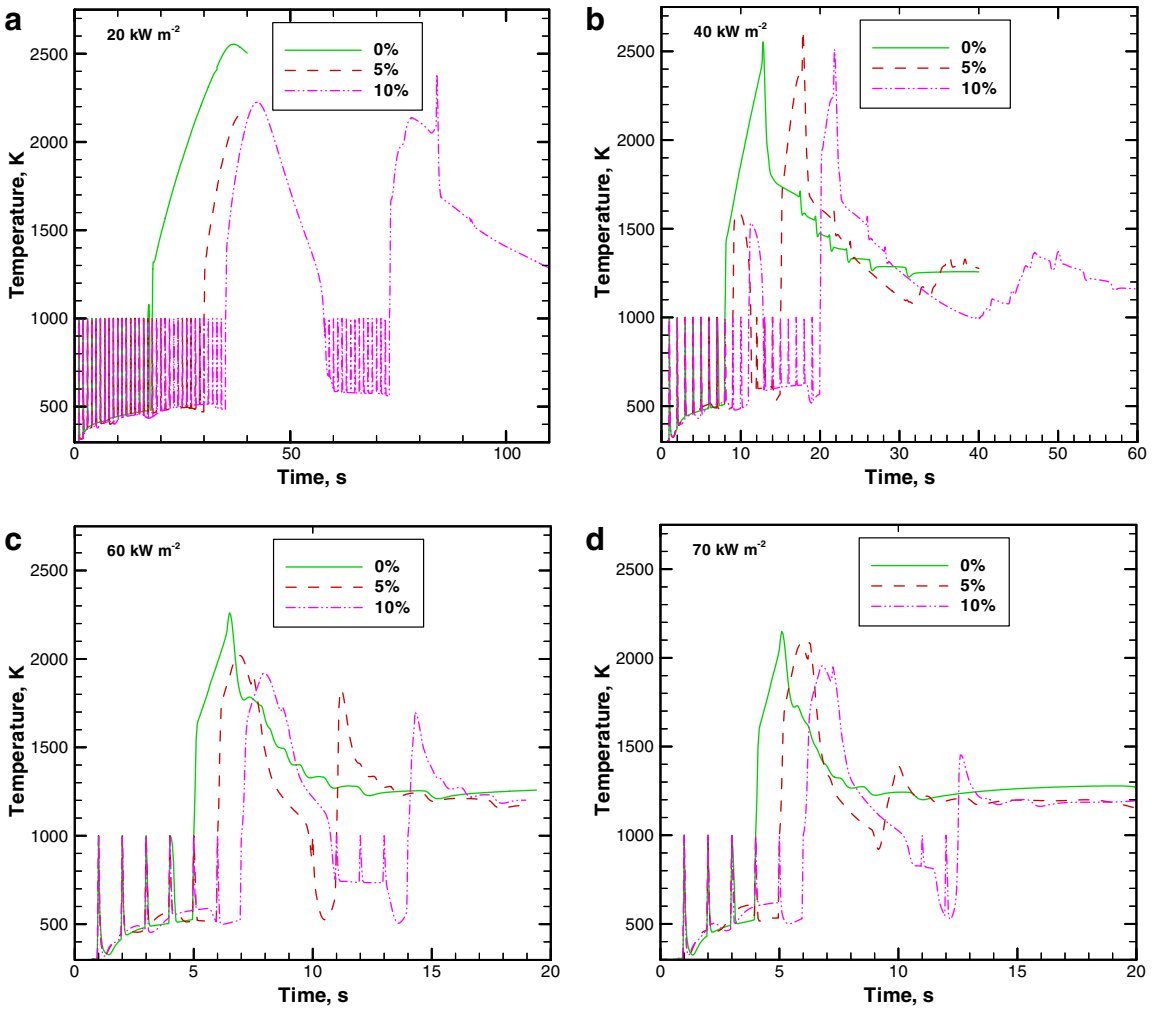

Fig. 3. Transient temperature development at the pilot position with initial moisture contents of 0%, 5% and 10% for irradiance: (a) 20 kW m^{-2}, (b) 40 kW m^{-2}, (c) 60 kW m^{-2} and (d) 70 kW m^{-2}.

the piloted ignition time increased with moisture content. Similar trends were also observed with the other investigations of wood with different irradiances from the conical heater and various initial moisture contents. An increase in the initial moisture content of wood caused a lengthening of the pilot ignition time at any irradiance level. Nevertheless, an increase in irradiance levels from the conical heater resulted in a reduction of the ignition time.

Table 1 presents the comparison between the predicted piloted ignition times and experimental results of Shields et al. [16]. During the experiments, the wood specimens were pre-conditioned carefully in a controlled environment

Table 1
Comparison of the computed pilot ignition times with the measured pilot ignition times[a]

Irradiance (kW m^{-2})	Computed pilot ignition time (s) % Initial moisture content			Measured pilot ignition time (s)[a]	
	0%	5%	10%	Spark[b]	Gas[c]
20	18	30	73	306–405	145–437
40	8	15	20	19–34	20–29
60	5	11	14	6–12	6–11
70	4	9	12	4–11	6–12

[a] Experimental ignition times for piloted ignitions of wood of a moisture content of 10% with an electric spark or gas pilot flame as reported by Shields et al. [16].
[b] Electric spark pilot source by means of high voltage across electrodes.
[c] Gas pilot source by means of a small naked flame.

of a temperature of 23 °C and a relative humidity of 50% before performing the pilot ignition experiments. Although the initial moisture contents of the sample were not reported, in this current study, the average initial moisture contents of samples are estimated to be 10% according to the formula of Skaar [29]. The predicted pilot ignition time was predicted to be 20 s for the irradiance 40 kW m^{-2}. The prediction agreed well within the range of experimentally determined pilot ignition times of 19–34 s and 20–29 s for spark and gas pilot ignition sources, respectively. For irradiance 60 kW m^{-2}, the predicted pilot ignition time was 14 s and it was just marginally out of the range of the reported values of 6–12 s and 6–11 s for spark and gas pilot ignition source. At the irradiance 70 kW m^{-2}, the predicted pilot ignition time was 12 s that was within the range of 6–12 s for the gas pilot ignition source from the experiments. However, the pilot ignition at irradiance 20 kW m^{-2} was predicted to be 73 s, which was considerably out of the range of the reported values. This discrepancy was most probably be attributed to the inadequacy of a first order reaction to describe the gas combustion and the lack of considerations of soot formation and gas radiant heat transfer in the gas phase combustion model. Also, the volatile gases produced from the pyrolysis of wood were assumed to contain pure fuel (100% combustible gas) with an empirical chemical formula of CH_2O. In a similar study by Tzeng and Atreya [21] through their one-dimensional pilot ignition model, the percentage of combustible gases was assumed to be as low as 20% of the total volatile gases produced in the pyrolysis, in order to improve their predictions. This was found to be important when the irradiance level was as low as 20 kW m^{-2}. Although such an adjustment could improved the predicted pilot ignition time, the transient values of the percentage of combustible gases were not verified by experiments and thus, considered to be artificial. Therefore, this adjustment was not pursued here.

4.2. Temperature, velocity and species concentration field

Owing to the axisymmetric nature of the solution, it was sufficient to illustrate the fluid flow, heat transfer and combustion characteristics only half of the elevation. Fig. 4 presents the computed temperature contours (on the left) and velocity vectors (on the right) while Fig. 5 shows the contours of mass fractions of fuel (on the left) and oxygen (on the right) for irradiance 40 kW m^{-2} with 10% initial moisture content, at 10 s time interval between 5 and 55 s. Since similar observations were also found with the computed results for the pilot ignition and combustion of wood with different initial moisture contents and irradiances of 20, 60 and 70 kW m^{-2}; they will not be presented herein.

At 5 s, the results confirmed the absence of neither flashing nor ignition. The fuel rich region was found at the central core and surrounded by an oxygen rich region due to entrainment of ambient air (see Fig. 5a). Along the surface of the conical heater, the temperature was above 900 K, which was close to the cone heater temperature of 988 K at 40 kW m^{-2} irradiance heat flux. The temperature contours reflected the entrainment of cool ambient air at the side and bottom inlet regions due to the buoyancy-induced flow developed by both the conical heater itself and the heated wood surface. At the pilot position, a high temperature zone was observed simulating the pilot source being turned on with a localised, short-lived combustion. However, the combustion process was not sustained because of the lack of gas volatiles which was confirmed by the fuel mass fraction distribution in Fig. 5a. The velocity profile indicated two peaks – one above the pilot point on the axis and the other in the immediate vicinity of the conical heater.

A gradually developing fuel rich region above the wood was found as the temperature of wood increased during the period from 5 to 20 s. The temperature and velocity distributions remained steady right up to 20 s. Although flashing occurred between 11 and 13 s, the amount of heat generated within this short period was unsustainable for combustion because of the buoyant flow having sufficient drag to carry the heat away. Nevertheless, as the temperature increased at the wood surface, more fuel was produced to replenish the burned fuel at the pilot ignition location and ignition occurred at 20 s with sustainable combustion of the gas volatiles. The isotherms illustrated a central core of high temperatures above the wood with the highest computed temperature predicted around 1900 K. This temperature representing a zone of rapid combustion in the gas phase was much higher than those found in the actual combustion of wood because of the absence the gas radiant heat absorption and soot formation in the gas phase model. The strong buoyancy due to the fire increased the velocities at the central axial region in the flow field to substantially higher values than those due to the conical heater at the sides.

At 25 s (5 s after ignition), rapid consumption of the fuel occurred at the central combustion core. In this region, the fuel mass fraction was as low as 0.005. Owing to the growth of fire above the wood, the combustion zone expanded radially outwards towards the edge of the wood. The fuel-rich region immediately above to the wood surface has extended upwards indicating a stronger fuel supply due to the increasing heat feeding back to the wood surface after ignition. Rapid combustion occurred as the fuel migrated upwards and entered the combustion zone. A steady fire was established as illustrated by the temperature and velocity distributions along with a central core of high fuel but low oxygen concentration between 25 and 55 s. The fuel mass fraction contour of 0.005 formed a distinct edge that indicated the flame front. As indicated by the isotherms above 1050 K at 55 s, the combustion zone covered most but not all the wood surface. This was evidenced by the ridge of fuel-rich gas near the edge of the wood in Fig. 5f where the combustion has not fully extended to the outer edge of the wood. Two velocity peaks corre-

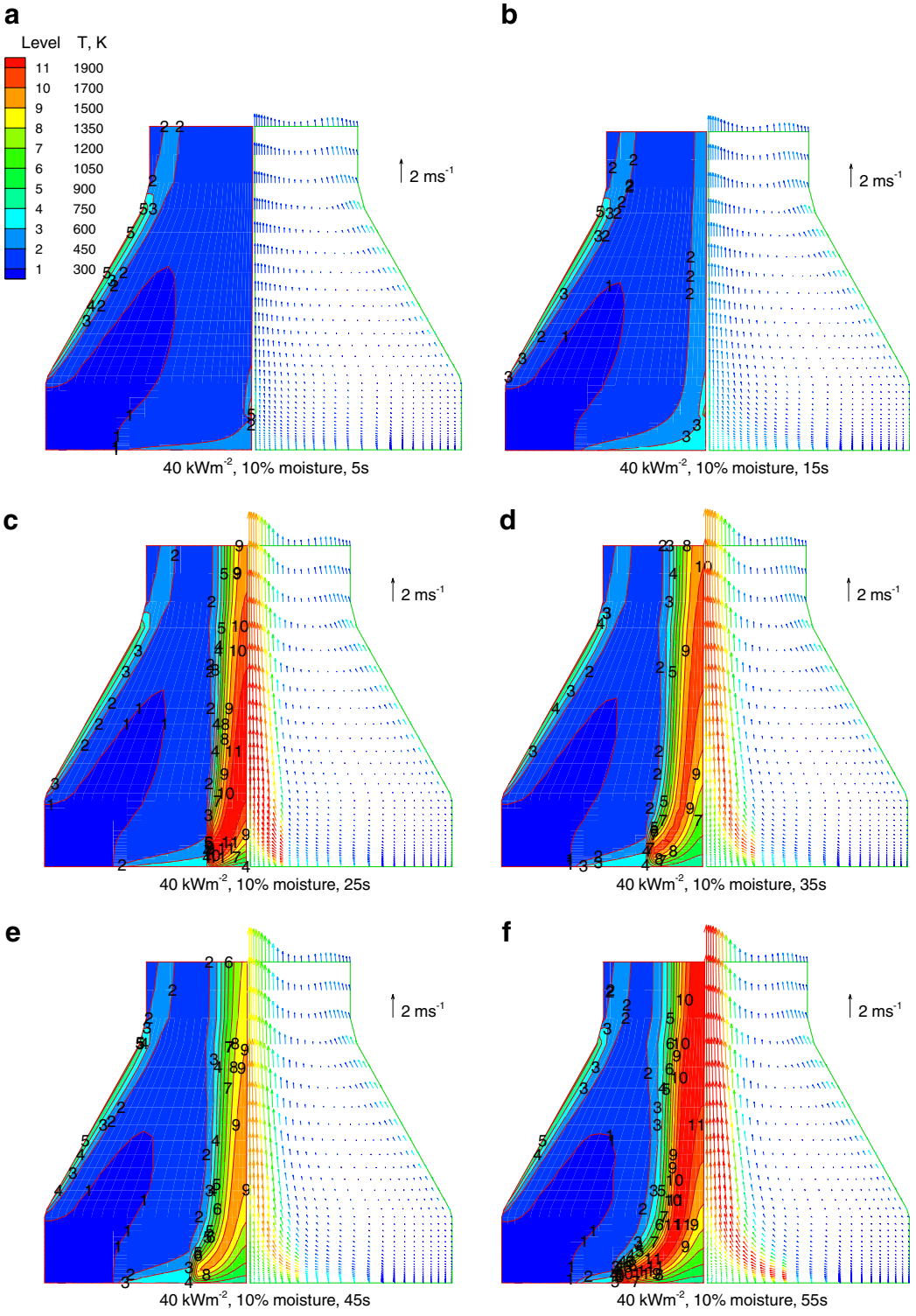

Fig. 4. Transient isotherms (left) and velocity vectors (right) for irradiance 40 kW m^{-2} with an initial moisture content of 10% at: (a) 5 s, (b) 15 s, (c) 25 s, (d) 35 s, (e) 45 s and (f) 55 s.

sponding to the buoyant flows were observed due to the fire and to the conical heater. The peak velocities remained almost the same as at 25 s. However, following the radial growth of the fire, the high velocity central axial core due to the combustion also expanded radially.

4.3. Temperature history, evaporation of moisture and char fraction in wood

Fig. 6 demonstrates the distributions of temperature, char fraction ρ_c/ρ_w and moisture fraction ρ_m/ρ_w at various

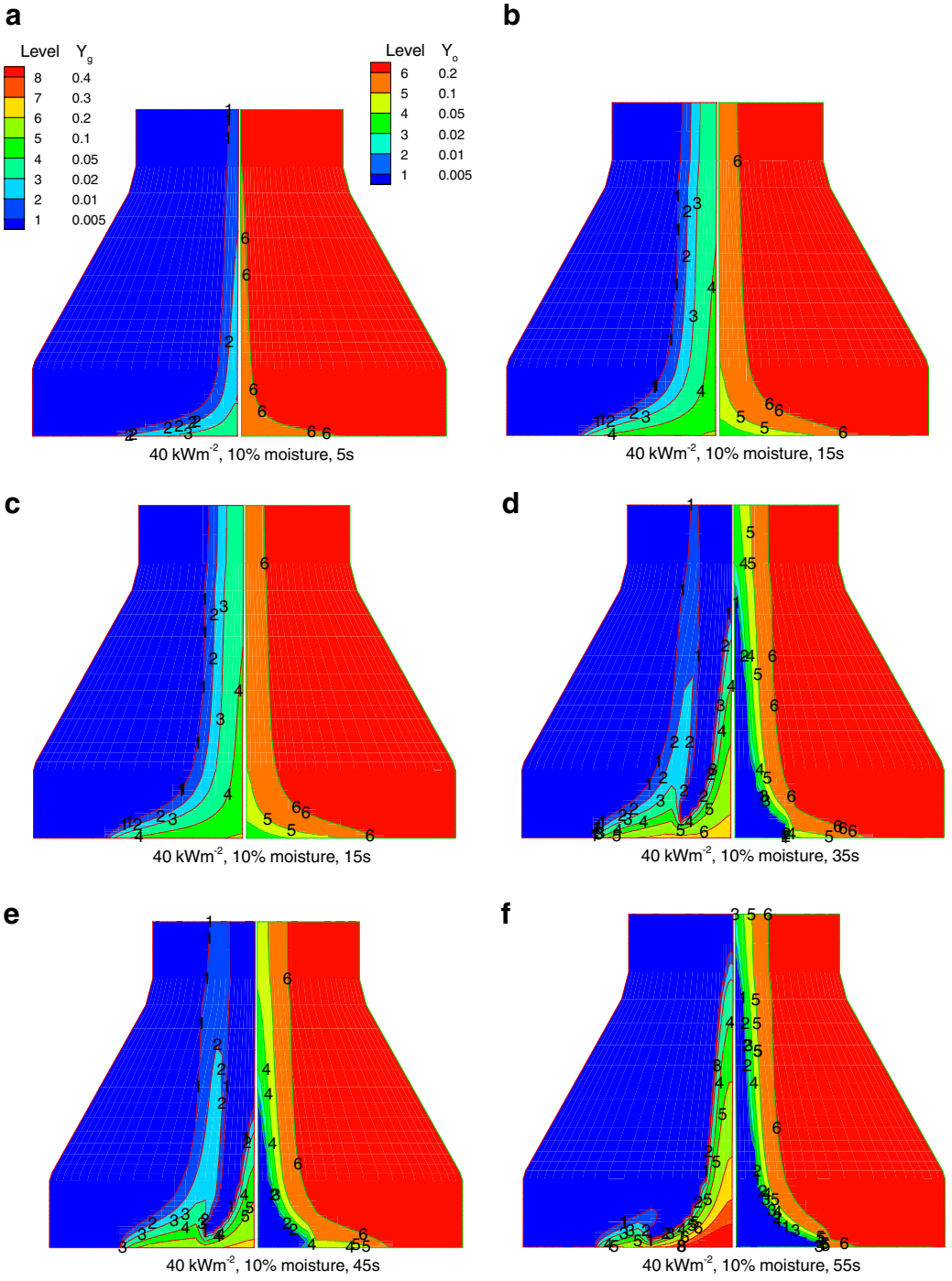

Fig. 5. Transient contours of mass fractions of fuel (left) and oxygen (right) for irradiance 40 kW m^{-2} with an initial moisture content of 10% at: (a) 5 s, (b) 15 s, (c) 25 s, (d) 35 s, (e) 45 s and (f) 55 s.

depths from 0.35 to 5.51 mm below the surface at the centre line of the wood at 40 kW m^{-2} irradiance and initial moisture content of 10%. Similar behaviours were also observed for initial moisture content of 0% and 5%. At a depth of 0.35 mm (just below the exposed surface of wood), the temperature increased continuously and gradually to a value of around 610 K. Shortly after piloted ignition and the development of sustained combustion above the wood, a sudden jump of the temperature was observed at around 12 s, which corresponded to the downward heat conduction for the combustion zone above the wood. Similar jumps of the temperature curves for the depth of 0.35 mm below the wood surface were also observed after ignition when the temperature reached around 610 K, which also indicated sustained combustion developing above the wood in the gas phase. Particularly for wet wood, there was a distinct change in the slopes of the curves corresponding to the depths of 0.35–3.28 mm, at

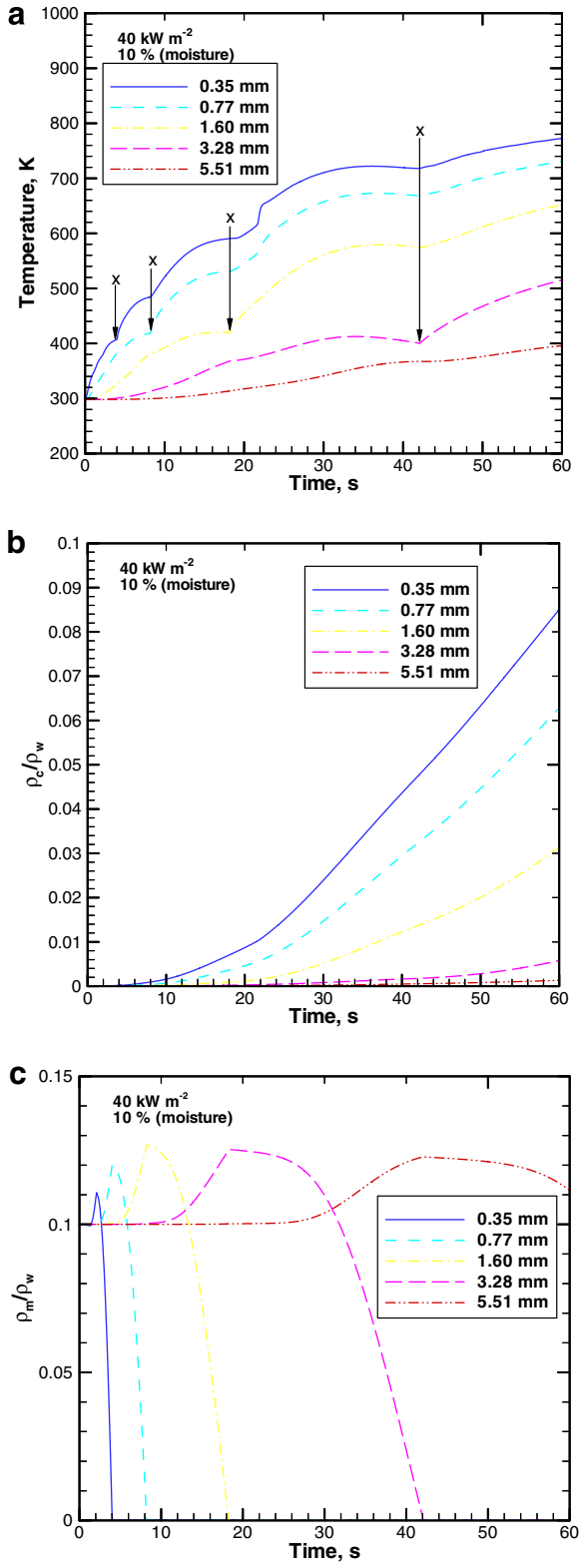

Fig. 6. Transient distributions at various depth below the surface at the centre of wood for irradiance 40 kW m^{-2} with initial moisture content of 10%: (a) Temperature, (b) Char fraction ρ_c/ρ_w and (c) moisture fraction ρ_m/ρ_w.

the points marked "×". Before "×", absorption of latent heat during evaporation of moisture reduced the rate of rise of temperature. Unlike commonly found ordinary vaporisation processes at ambient conditions where the pressure is normally constant (at atmospheric pressure), the pressure has a tendency to increase inside the wood due to the accumulation of trapped vapour in wood and the poor permeability of the porous wood substrate while undergoing vaporisation. During the vaporisation process inside the wood, temperature was still increasing but at a slower rate than that for dry wood. The vaporisation process generally began at 373 K and terminated at around 420 K. After "×", the rate of rise of temperature increased due to the evaporation of the moisture. Some evaporation was noticeable at 5.51 mm as indicated by the slight decrease of slope of the temperature curve. The process was not completed during the simulation and "×" was not marked on that temperature curve. The computed temperatures at 40 kW m^{-2} irradiance with initial moisture contents of 5% and 10% agreed qualitatively with the measured transient temperatures of Blackshear and Kanury [30], Lee and Diehl [31] and Tran and White [32]. In their experiments, thermocouples were inserted at various depths in wood specimens for the measurement of transient temperature history of the pyrolysing wood. All the transient temperature curves demonstrated clearly a plateau around 100 °C, which corresponded to the evaporation of the moisture in wood.

For the particular case of 10% initial moisture content, the rate of generation of char was relatively slower at the beginning even at the depth of 0.35 mm, until the temperature at that point exceeded 500 °C at about 10 s when the pyrolysis rate subsequently inside the wood dominated. There was a slight increase in the rate of char formation as observed from the small but noticeable increase in gradient of the char fraction curve at 21 s. This was a result of the additional heat input to the wood from the combustion zone above it due to ignition at 20 s (see Table 1). The presence of initial moisture in the wood and its evaporation also contribute to the slower rate of pyrolysis and hence production of char in the starting period of heating. Also, an increase in moisture content was seen occurring before evaporation began at all positions. This was due to some of the vapour produced in the higher temperature zone nearer the surface of the wood that has migrated downwards due to a pressure gradient towards the cooler regions of the wood where the condensation of vapour to liquid occurred. At a depth of 0.35 mm, the moisture content increased until the onset of the evaporation which occurred at 2 s. The evaporation at this point ceased at 4 s when the available moisture was totally consumed. Upon the completion of evaporation at this depth at 4 s, the moisture at 0.77 mm began to evaporate. As the evaporation continued between 2 and 4 s, the slope of temperature curve gradually decreased indicating the absorption of heat due to vaporization. This change of slope of the temperature curve was more obvious at deeper positions in the wood (0.77–5.51 mm) where the evaporation processes occurred much later and took a longer time to complete. Also, the lengthened duration of the evaporation at the inner parts

of the wood was a result of the reduction of the rate of heat transfer mainly due to the convective cooling effects of the emerging vapour and possibly volatile gases from the wood as well as the formation of the insulating char layer at the surface of the wood. The starting and ending times for the evaporation process indicated that the evaporation occurred at retarded rates with increasing depth.

5. Conclusion

A 3-D mathematical model based on the non-orthogonal curvilinear coordinate system to simulate the geometry and flow filed within a cone calorimeter has been demonstrated. A model was developed for the heat transfer and pyrolysis within dry and wet wood specimens subjected to radiation emitted by the cone, and a model was developed for the mixing and pilot ignition of the released gas volatiles with the air above the wood sample. The formulation of the wood pyrolysis model has been described in Part 1 of this two-part study, which included detailed considerations of the evaporation of moisture, anisotropic and variable properties, and pressure driven internal convection of gases in wood.

Predicted results showing the transient thermal response and the combustion phenomenon of the wood corresponded to typically observed cone calorimeter experiments. During the computations, the pilot has been simulated numerically and ignition criteria such as critical surface temperature and critical mass flux were not required. The effects of initial moisture content on ignition time showed that higher initial moisture content delayed ignition. Flashing ignitions were also observed for wood with initial moisture contents of 5% and 10%. The growth of the fire and the pyrolysis of wood are described. The predicted flame shapes, which are indicated by the computed temperature fields, demonstrated the transient growth of the fire and pyrolysis processes of wood. The numerically predicted pilot ignition times over a range of external irradiance fluxes from 20 to 70 $\mathrm{kW\,m^{-2}}$ and initial moisture contents of 0%, 5% and 10% were found to compare well with experimental measurements. However, the predicted pilot ignition at irradiance 20 $\mathrm{kW\,m^{-2}}$ was considerably lower than the experimentally reported values. This discrepancy was most probably be attributed to the inadequacy of a first order reaction to describe the gas combustion and the lack of considerations of soot formation and gas radiant heat transfer in the gas phase combustion model.

It has been demonstrated in this paper that the current 3-D model for pyrolysis of wet wood coupled with the gas phase combustion can be used to describe the sophisticated chemical and physical processes associated with the pyrolysis of wood in complex geometrical configurations. Significant improved predictions to the phenomena can be better attained with the inclusion of suitable models for the radiant heat transfer and soot formation and multiple reactions accommodated within the gas phase combustion model to better described the chemistry of combustion.

References

[1] ASTM E1354, Standard test method for heat and visible smoke release rates for materials and products using an oxygen calorimeter, Annual Books of ASTM Standards, ASTM, Philadelphia, PA, 1990.
[2] ISO 5660, Fire tests, reaction to fire, rate of heat release from building products, ISO, Geneva, Switzerland, 1993.
[3] R.D. Peacock, R.W. Bukowski, S.H. Markos, Evaluation of passenger train car materials in the cone calorimeter, Fire Mater. 23 (1999) 53–62.
[4] K.-C. Tsai, D. Drysdale, Using the cone calorimeter data for the prediction of fire hazard, Fire Safety J. 37 (2002) 697–706.
[5] M. Delichatsios, B. Paroz, A. Bhargava, Flammability properties for charring materials, Fire Safety J. 38 (2003) 219–228.
[6] C. Di Blasi, S. Crescitelli, G. Russo, G. Cinque, Numerical models of ignition processes of polymeric materials including gas-phase absorption of radiation, Comb. Flame 83 (1991) 333–344.
[7] M.I. Nelson, J. Brindley, A. Mcintosh, A mathematical model of ignition in the cone calorimeter, Comb. Sci. Tech. 5104 (1995) 33–54.
[8] J. Rychly, L. Costa, Modelling of polymer ignition and burning adopted for cone calorimeter measurements. The correlation between the rate of heat release and oxygen index, Fire Mater. 19 (1995) 215–240.
[9] B.T. Rhodes, J.G. Qunintiere, Burning rate and flame heat flux for PMMA in a cone calorimeter 26 (1996) 221–240.
[10] C. Brescianni, G.H. Yeoh, V. Chandrasekaran, R.K.K. Yuen, A numerical model for pilot ignition of PMMA in a cone calorimeter, Comb. Sci. Tech. 120 (1997) 321–345.
[11] T.-H. Tsai, M.-J. Li, I.-Y. Shih, R. Jih, S.-C. Wong, Experimental and numerical study of a autoignition and pilot ignition of PMMA plates in a cone calorimeter, Comb. Flame 124 (2001) 466–480.
[12] B. Moghtaderi, V. Novozhilov, D.F. Fletcher, J.H. Kent, An integral model for the transient pyrolysis of solid materials, Fire Mater. 21 (1997) 7–16.
[13] B. Moghtaderi, V. Novozhilov, D.F. Fletcher, J.H. Kent, Mathematical modelling of the piloted ignition of wet wood using the heat-balance integral method, J. Appl. Fire Sci. 6 (1997) 91–107.
[14] M.J. Spearpoint, J.G. Qunintiere, Predicting the piloted ignition of wood in the cone calorimeter using an integral model – effect of species, grain orientation and heat flux, Fire Safety J. 36 (2001) 391–415.
[15] V. Novozhilov, B. Moghtaderi, D.F. Fletcher, J.H. Kent, Computational fluid dynamics modelling of wood combustion, Fire Safety J. 27 (1996) 69–84.
[16] T.J. Shields, W.H. Silcock, J.J. Murray, The effects of geometry and ignition mode on ignition times obtained using a cone calorimeter and ISO ignitability apparatus, Fire Mater. 17 (1993) 25–32.
[17] A. Bejan, Heat Transfer, John Wiley & Sons, New York, 1993.
[18] K.K. Kuo, Principles of Combustion, John Wiley & Sons, New York, 1986.
[19] R. Siegel, J.R. Howell, Thermal Radiation Heat Transfer, McGraw-Hill, New York, 1992.
[20] A. Atreya, Pyrolysis, Ignition and Fire Spread on Horizontal Surfaces of Wood, Ph.D. Thesis, Harvard University, 1983.
[21] L.S. Tzeng, A. Atreya, Theoretical Investigation of Pilot Ignition of Wood, NIST Report No: NIST-GCR-91-595, NIST, Building and Fire Research Laboratory, 1991.
[22] D. Drysdale, An Introduction to Fire Dynamics, John Wiley & Sons, New York, 1985.
[23] C.K. Westbrook, F.L. Dryer, Simplified reaction mechanisms for the oxidation of hydrocarbon fuels in flames, Comb. Sci. Tech. 27 (1981) 31–43.
[24] H.L. Stone, Iterative solution of implicit approximations of multi-dimensional partial differential equations, SIAM J. Numer. Anal. 5 (1968) 530–558.

[25] C.A.J. Fletcher, Computational Techniques for Fluid Dynamics: Fundamental and General Techniques, Springer-Verlag, New York, 1991.
[26] S.S. Alves, J.L. Figueiredo, A model for pyrolysis of wet wood, Chem. Eng. Sci. 44 (1989) 2861–2869.
[27] B. Fredlund, Modelling of heat and mass transfers in wood structures during fire, Fire Safety J. 20 (1993) 39–69.
[28] C. Di Blasi, On the influence of physical processes on the transient pyrolysis of cellulosic samples, Int. Symp. Fire Safety Sci. (1994) 229–240.
[29] C. Skaar, Wood-Water Relations, Springer-Verlag, New York, 1988.
[30] P.L. Blackshear Jr., A.M. Kanury, On the combustion of wood I: A scale effect in pyrolysis of solids, Comb. Sci. Tech. 2 (1970) 1–4.
[31] C.K. Lee, J.H. Diehl, Combustion of irradiated dry and wet oak, Comb. Flame 42 (1981) 123–138.
[32] C.H. Tran, R.H. White, Burning rate of solid wood measured in a heat release rate calorimeter, Fire Mater. 16 (1992) 197–206.